Tunable Hot-Electron Transfer Within a Single Core-Shell Nanowire

Guannan Chen, Eric M. Gallo, Oren D. Leaffer, Terrence McGuckin, Paola Prete, Nico Lovergine, and Jonathan E. Spanier

Phys. Rev. Lett. **107**, 156802 — Published 5 October 2011

DOI: 10.1103/PhysRevLett.107.156802

Tunable hot-electron transfer within a single core-shell nanowire

Guannan Chen,[1] Eric M. Gallo,[1] Oren D. Leaffer,[1] Terrence McGuckin,[1] Paola Prete,[2], Nico Lovergine,[3] and Jonathan E. Spanier[1]

[1]*Department of Materials Science and Engineering, Drexel University, Philadelphia, PA 19104 USA;*

[2]*Istituto per la Microelettronica e Microsistemi (IMM), Consiglio Nazionale delle Ricerche (CNR), Lecce, Italy;*

[3]*Department of Innovation Engineering, University of Salento, Lecce, Italy**

(Dated: August 8, 2011)

Abstract

We report hot photo-excited electron transfer across the co-axial interface of a cylindrical core-shell nanowire. Modulation of the transfer rates, manifested as a large tunability of the voltage onset of negative differential resistance and of voltage-current phase, is achieved using three different modes. Coupling of electrostatic gating, incident photon energy and incident photon intensity to transfer rates is facilitated by the combined influences of geometric confinement and heterojunction shape on hot electron transfer, and by electron-electron scattering rates that can be altered by varying the incident photon flux, with evidence of weak electron-phonon scattering. Dynamic manipulation of this transfer rate permits introduction and control of a continuously adjustable phase delay of up to $\sim$130° within a single nanometer-scale device element.

*email:spanier@drexel.edu

Understanding the effects of finite size and dimensionality on the interaction of light with semiconductor nanostructures, e.g. local enhancement of electromagnetic fields[1], optical absorption[2], exciton dynamics[3], multi-exciton generation[4] and electron transfer across semiconductor heterostructures[5] is central to identifying and exploiting[6–10] novel modes of efficient conversion and transfer of energy. However, insight into the physics of hot electron cooling and transfer across electrically-interfaced heterojunctions, realized and studied extensively in real space transfer (RST) devices, has been limited to planar interfaces in which local carrier densities are bounded principally by excited state lifetimes rather than finite geometric or mesoscopic symmetry considerations.

Here we report tunable hot electron transfer of photo-excited electrons across the co-axial interface of a core-shell nanowire. The rate of RST in the co-axial nanowire geometry can be tuned using three different mechanisms and is manifest as a tunability of the negative differential resistance, where the dependence on transfer rate on an energy relaxation length scale is expected to possesses a stronger power law dependence in the co-axial geometry than in a planar geometry. Tunability using incident light wavelength indicates an ultrafast carrier dynamic, relevant to the study of hot carrier cooling. The controlled variation of incident photon flux on electron-electron interactions represents a promising means of investigating momentum relaxation and distribution in geometrically confined nanostructures. The introduction of a single nanoscale element possessing electrically- and optically-tunable complex impedance opens the possibility of assembling integrated circuits, including oscillators, amplifiers[11], phase-shifters, frequency multipliers, phase-locked loops, and laser switches[12] using fewer and far smaller elements, and with the versatility of a highly local optical interface[8, 13–15].

Core-shell nanowires (CSNWs) each composed of a GaAs core and an $Al_{0.33}Ga_{0.67}As$ shell were grown via metallorganic vapor phase epitaxy without additional introduction of dopant. CSNWs were dispersed onto a 200-nm thick thermally-grown SiO_2 film on an electrically-contacted Si(100) substrate for electrostatic gating, and electron beam lithography was used to define electrical contacts directly to the core near each end of the CSNWs. The NW cores possess nearly intrinsic character at 300K: they are slightly p-type on the basis of recent demonstration of gate modulation of conductance within GaAs NWs without a shell[16], consistent with the unintentional doping (C) from precursor molecules[17], and thereby substantially suppressing the scattering by ionized dopants in

the GaAs NW cores. We estimate the alloy composition x to be 0.33 in our $Al_xGa_{1-x}As$ shells based on the results of Voigt lineshape fitting-based determination of the positions of the GaAs TO and LO phonon modes, and AlAs- and GaAs-like TO and LO modes for the $Al_xGa_{1-x}As$ alloy in the Raman spectra collected from the core-shell NWs, thus permitting extraction of values for x(Al). Values obtained for x were consistent (within a few %) with those obtained from photoluminescence spectroscopy. The shells are expected to be weakly n-type due to unintentional doping (Si) from the Al-based precursor.

The CSNWs exhibit significant photocurrent sensitivity ($\sim$0.1 μA/W) at 300K in their low bias voltage response to either monochromatic laser or broadband illumination as evidenced by remarkably small dark currents (< 50 fA), amounting to more than three orders of magnitude in the linear variation in photocurrent. A nearly linear photocurrent-voltage relationship for small DC bias V_{bias} at 300K indicates photo-generated carriers encounter a negligibly small barrier when collected. However, application of larger bias reveals NDR in the photocurrent, where a threshold voltage V_{th} is defined by onset of the NDR. For $V_{bias} \approx V_{th}$ photo-excited electrons in the GaAs NW core can acquire sufficient energy from the large component of E parallel to the NW axis, exceeding the GaAs-$Al_{0.33}Ga_{0.67}As$ conduction band offset ($\Delta E_c \approx 0.255$ eV[18]) and undergo real-space transfer (RST)[19–23] into the shell (Fig. 1(b)). For $V > V_{th}$, the curve bends down, and with a further increase in the applied electric field E, the slope of the curve becomes nearly zero and the photocurrent is saturated.

For sufficiently large E, RST of photo-excited electrons from the higher electron mobility NW core to the lower-mobility and wider-gap shell, and the accompanying observation of NDR in photocurrent density $J_{\hbar\omega}$ can be described by $dJ_{\hbar\omega}/dE = q\delta n[\mu_1 - f\Delta\mu - (df/dE)\Delta\mu E]$ where $\Delta\mu = \mu_1 - \mu_2$, μ_1 and μ_2 denote GaAs core and $Al_{0.33}Ga_{0.67}As$ shell electron mobilities (bulk values are $\sim$8000 $cm^2V^{-1}s^{-1}$[11] and $\leq$ 500 $cm^2V^{-1}s^{-1}$[11]), respectively, δn is the concentration of photo-induced electrons within the GaAs core, and f is an E field-dependent fraction of carriers photo-excited within the core that reach the shell. A peak in the current is expected when $dJ_{\hbar\omega}/dE = 0$, i.e. $\mu_1/\Delta\mu = f + Edf/dE$, from which estimates of f at V_{th} can be obtained by numerically solving the above ($0.23 \lesssim f \lesssim 0.45$). Due to the complexity of solving the Boltzmann transport equation involving RST, Monte-Carlo simulations are usually applied to simulate the velocity $v - E$ relationship[19, 24, 25]. Assuming E is constant along the axis of the

NW, we estimate that our measured V_{th} corresponds to $E \approx 10$ kV/cm. This is comparable to the value of ~ 3 kV/cm in bulk structures calculated by Monte Carlo simulations and obtained experimentally[21, 24]; an increase is consistent with predictions of increases in threshold voltage for decreased dimensionality from bulk to two dimensions[19].

On what basis can the observed NDR in photocurrent be attributed to RST? RST is directly related to the energy that a hot electron accrues from the incident photon energy. Incident radiation with a larger energy difference ($E_{\hbar\omega} - E_{g,\mathrm{GaAs}}$) will generate a broader distribution of electron energies in excess of $E_{g,\mathrm{GaAs}}$ (and higher electron temperatures), requiring a lower electric field to undergo RST. In fact, we verified this dependence by observing a shift in V_{th} with incident photon energy, i.e. $dV_{th}/dE_{\hbar\omega} < 0$ (Fig. 2(a)). In addition to its potential application for a wavelength-selective non-linear device element, significantly, this finding also indicates that the transit time for electrons to reach RST threshold is comparable to, or shorter than, the hot electron cooling time, indicating the potential for this device in high-frequency RST-based nano-scale optoelectronics.

V_{th} depends on ΔE_c and thus we propose that the rate of RST and the field associated with its onset in a CSNW can be manipulated via electrostatic gating of the entire length of the CSNW, given its radial proximity to the gate electrode. Measured photocurrent vs. V_{bias} with substrate gating demonstrates that V_{th} can be tuned by up to $\sim$50%, with $dV_{th}/dV_g < 0$, confirming that it is electrons (and not holes) in the GaAs core that are undergoing RST (Fig. 2(b)). The additional field contributed by $V_g > 0$ provides a radial component of momentum to the electrons in the GaAs core (transverse to the heterojunction) to enter the AlGaAs shell. Non-uniformity in the radial field distribution from gate coupling is expected: a maximum field is reached where the NW is in physical contact with the gate oxide[26].

The asymmetric NDR response of our devices to gating can be understood by considering the additional contribution to the overall capacitance owing to the NW shell-core interface in the form of a bipolar ($n - p$) junction-isolated channel. Electron transfer across the NW heterojunction under $V_g > 0$ is analogous to a negatively biased $p - n$ junction, in which saturation can be attained with small V_g. For $V_g < 0$, however, the bipolar channel is under positive bias and saturation is not observed for an appreciable range of V_g. A more detailed study of the extent of applicability of RST to observations of NDR on photocurrent in CSNWs should consider momentum and energy relaxation mechanisms

under E. However, on the basis of the strong electrostatic gating effect, of estimates of energy differences between the conduction band offset and transition energies associated with different conduction band minima in k-space, and of the observed excitation energy dependence of RST, we assert that it is much more energetically favorable for electrons to undergo RST than inter-valley transition(s)[18, 27, 28].

Under high E-field, electron-electron scattering contributes to randomizing energy gained from the E-field along the channel, resulting in an increased momentum relaxation rate and a shorter timescale for the carrier distribution to reach steady-state[19, 29, 30]. This is particularly beneficial for RST since the randomization process enables a larger fraction of transporting electrons in the channel to accrue a sufficient radial component of momentum to transfer across the interface.

Based on the principle that electron-electron scattering rate is a function of carrier concentration (in our case δn) we investigated the effect of this scattering rate on the onset of RST by varying the optical excitation intensity $I_{\hbar\omega}$. Significantly, we observe that V_{th} can *also* be tuned by $\sim$50%, with $dV_{th}/dI_{\hbar\omega} < 0$ over the range $0 \leq I_{\hbar\omega} \leq 14.1$ mW/cm^2 (Fig. 2(c)). Below a threshold excitation intensity however, the NDR feature is diminished, likely due to insufficient electron-electron scattering.

We rule out the possibility that the observed NDR is due to an unintended and unconfirmed presence of a tunnel barrier in our devices: our experimental results and *a priori* knowledge that the GaAs NW cores are very weakly p-type[16], taken together with our estimate of the peak instantaneous net excess carrier concentration[31] under our experimental conditions ($\delta n = 7.0\times10^{17}$ cm^{-3}[32]), and the absence of an appreciable thermal contribution, indicate that a tunneling process cannot explain the observed NDR feature in the photocurrent and its tunability with electrostatic gating and incident photon flux.

We investigated the temperature dependence of the photocurrent in our CSNWs from 300K to 4.2K. The strong NDR feature can also be seen at 4.2K under higher power monochromatic (0.33 mW) laser illumination, where nA-scale photocurrent and a more than 2:1 peak-to-valley photocurrent ratio are observed (Fig. 3(a)). While a decrease in the low-bias photo-conductance $G_{\hbar\omega}$ under lamp illumination for decreasing temperature T from 300K to 160K is seen, there is a remarkable absence of systematic variation in $G_{\hbar\omega}$ over the range from $\sim$160K to 4.2K (Fig. 3(b). These results indicate that, for $T \lesssim 160$K,

photo-excited carriers are not appreciably scattered by phonons in these devices.

We compare the probability of hot electrons to undergo RST in the cylindrical core-shell NW geometry to that for a planar structure, i.e. a thin layer of GaAs sandwiched between AlGaAs above and below it. Electron-electron scattering randomizes the momentum distribution while not changing the electron drift velocity. Assuming that the NW diameter ($2R$) and film thickness (t) in the planar structure are each small in relation to the absorption depth (i.e. the photo-excited electrons are uniformly distributed within the GaAs NW core or thin film layer) and defining an energy relaxation length L within which (all) hot electrons lose energy when entering the AlGaAs shell (or film), the probability of hot electrons created within the GaAs NW core undergoing RST (and the relative degree of tunability) is, to leading order in L, stronger ($\sim L^2$) than that for the planar geometry ($\sim L$). (Supplemental Materials)

We describe how the CSNW can be operated as an electrically- or optically-controllable non-linear nanoscale device element. For example, introduction of an ac modulation to V_{bias} at frequency ω about selected values of V_{th} defined by different values of incident optical intensity, we demonstrate full-wave rectification as seen by modulation frequency doubling, and tunability of its maximum along the bias voltage axis (Fig. 4(a)). For fixed incident power, the phase difference (between that of the ac voltage applied to the sample leads and the generated ac photocurrent) $\Delta\phi$ can be tuned continuously by bias voltage with $d\phi/dV \approx 130°/\mathrm{V}$ (Fig. 4(b)), demonstrating the potential for these CSNW devices as programmable phase delay elements and for use in frequency multiplication. Further, the 2ω current response to an sequence of arbitrary-amplitude light pulses incident upon the CSNW device under ac bias voltage (Fig. 4(c)) demonstrates optical amplitude control of nonlinearity in photocurrent.

The introduction of a single nanoscale element possessing electrically- and optically-tunable complex impedance opens the possibility of assembling integrated circuits, including oscillators, amplifiers[11], phase-shifters, frequency multipliers, phase-locked loops, and laser switches[12] using fewer and far smaller elements, and with the versatility of a highly local optical interface[8, 13–15]. While challenges owing to the effects of parasitic capacitance from the substrate must be addressed, we propose that, based on our observation of tunable frequency doubling at 1 kHz and on the inherent relaxation timescales for RST of $\sim 10^{-12}$ sec.[19], practical GHz-range single nanowire devices exhibiting tunable phase should be

within reach, particularly given recently reported evidence of intrinsic picosecond-scale response time characteristics of these CSNWs[33]. Finally, the dynamic control of hot-electron transfer rates in nano-scale heterojunctions as reported here is relevant for novel photovoltaic devices: a significant reduction in the timescale of hot electron transfer from semiconductor nanocrystals was demonstrated recently[34] renewing intense interest in efforts to approach the theoretical limit of quantum efficiency for hot-electron transfer that far exceeds[35] the Shockley-Queisser limit[36].

The authors thank Cherie Kagan and Kevin Siegl for comments, and Ilio Miccoli, Joan Burger, and Michael Coster for assistance with growth of the NWs and device fabrication. Work at Drexel was supported by the NSF (DMR-0907381) and by the U.S. Army Research Office (W911NF-08-1-0067).

Supplemental Materials: Description of device fabrication; calculation of transfer fraction f; geometric considerations for comparing RST in cylindrical NW and planar hetero-junctions; demonstration of optical modulation under Ti:S laser; device response under laser irradiation and at 1 kHz; optical polarization effect.

[1] L. Cao, B. Nabet, and J.E. Spanier, Phys. Rev. Lett. **96**, 157402 (2006).

[2] L. Cao, J. S. White, J. S. Park, J. A. Schuller, B. M. Clemens, and M.L. Brongersma, Nat. Mater. **8**, 643-647 (2009).

[3] M. Wagner, H. Schneider, D. Stehr, S. Winnerl, A. M. Andrews, S. Schartner, G. Strasser, and M. Helm, Phys. Rev. Lett. **105**, 167401 (2010).

[4] N.M. Gabor, Z. Zhong, K. Bosnik, J. Park, and P. L. McEuen, Science **325**, 1367-1371 (2009).

[5] J.B. Sambur, T. Novet, and B. A. Parkinson, Science **330**, 63-66 (2010).

[6] J. Xiang, W. Lu, Y. Lu, H. Yan, and C.M. Lieber, Nature **441**, 489-493 (2006).

[7] R. Yan, D. Gargas, and P. Yang, Nature Photonics **3**, 569-576 (2009).

[8] R.F. Oulton, V.J. Sorger, T. Zentgraf, R.-M. Ma, C. Gladden, L. Dai, G. Bartal, P. Lalanne, and X. Zhang, Nature **461**, 629 (2009).

[9] M.P. van Kouwen, M.E. Reimer, A.W. Hidma, M.H.M. van Weert, R.E. Algra, E.P.A.M. Bakkers, L.P. Kouwenhoven, and V. Zwiller, Nano Lett. **10**, 1817 (2010).

[10] H. Yan, H.S. Choe, S.W. Nam, Y. Hu, S. Das, J.F. Klemic, J.C. Ellenbogen, and C.M. Lieber, Nature **470**, 240 (2011).

[11] S.M. Sze, Physics of semiconductor devices, John Wiley & Sons, (1981).

[12] J.F. Whitaker, G.A. Mourou, T.C.L.G. Sollner, and W.D. Goodhue, Appl. Phys. Lett. **53**, 385 (1988).

[13] X. Duan, Y. Huang, R. Agarwal, and C.M. Lieber, Nature **421**, 241-245 (2003).

[14] F. Qian, Y. Li, H.G. Park, Y. Dong, Z.L. Wang, and C.M. Lieber, Nature Mater. **7**, 701-706 (2008).

[15] J. Claudon, J. Bleuse, N.S. Malik, M. Bazin, P. Jaffrennou, N. Gregersen, C. Sauvan, P. Lalanne, and J.-M. Gerard, Nature Photonics **3**, 174-177 (2010).

[16] G. Chen, E.M.Gallo, J.Burger, B.Nabet, P.Prete, N.Lovergine, and J.E.Spanier, Appl. Phys. Lett. **96**, 223107 (2010).

[17] P. Prete, F. Marzo, P. Paiano, N. Lovergine, G. Salviati, L. Lazzarini, and T. Sekiguchi, J. Crystal Growth 310, 5114-5118 (2008).

[18] We compare the conduction band offset ΔE_c with the transition energies associated with different conduction band minima ($\Delta E_{\Gamma-L}$ (0.29 eV) and $\Delta E_{\Gamma-X}$ (0.48 eV)). We estimate the conduction band offset using $x = 0.33$ in the expression $0.7730x$ (for $x < 0.45$) $= 0.255$ eV.[27] An alternate estimate can be obtained by subtracting the measured or calculated values for valence band offset for this composition ($\Delta E_v \approx 0.134$ eV[28]) from the energy gap difference, i.e. $\Delta E_g = E_{g,\mathrm{Al_{0.33}Ga_{0.67}As}}$ (= 1.84 eV[27]) $- E_{g,\mathrm{GaAs}}$ (= 1.42 eV) = 0.42 eV, and thus $\Delta E_c = 0.285$ eV.

[19] K. Hess, H. Morkoç, H. Shichijo, and B. Streetman, Appl. Phys. Lett. **35**, 469 (1979).

[20] Z. Gribnikov, Soviet Physics - Semiconductors **6**, 1204-5 (1973).

[21] M. Keever, Appl. Phys. Lett. **38**, 36 (1981).

[22] S. Luryi, Appl. Phys. Lett. **58**, 1727 (1991).

[23] G.L. Belenky, P.A. Garbinski, S. Luryi, M. Mastrapasqua, A.Y. Cho, R.A. Hamm, T.R. Hayes, D.L. Sivco, and P.R. Smith, J. Appl. Phys. **73**, 8618 (1993).

[24] T. Glisson, J. Appl. Phys. **51**, 5445-5449 (1980).

[25] T. Wang, and K. Hess, J. Appl. Phys. **57**, 5336 (1985).

[26] D.R. Khanal and J. Wu, Nano Lett. **7**, 2778-2783 (2007).

[27] S. Adachi, J. Appl. Phys. **58**, R1 (1985).

[28] W. Mönch, Electronic properties of semiconductor interfaces, Springer: Berlin, Heidelberg, (2004).

[29] C. Jacoboni and L. Reggiani, Rev. Mod. Phys. **55**, 645 (1983).

[30] S.M. Goodnick and P. Lugli, Phys. Rev. B **37**, 2578 (1988).

[31] O. Demichel, M. Heiss, J. Bleuse, H. Mariette, and A. Fontcuberta i Morral, Appl. Phys. Lett. **97**, 201907 (2010).

[32] We estimate the optically-generated electron concentration δn by assuming here a one-dimensional steady state optical injection, the steady state condition $G = (S_n + \frac{D_n}{L_n})(\delta n)_0$ where $G = (P/\hbar\omega)A^{-1}$ cm^{-2}s^{-1}, P is the incident power of radiation of energy $\hbar\omega$, A is the Gaussian laser spot area, S_n is the surface recombination rate in cm s^{-1}, and D_n and L_n are the diffusion coefficient and diffusion length, respectively. Here, $G = 2.05\times10^{21}$ cm^{-2}s^{-1} for P = 10 mW, $\hbar\omega = 1.549$ eV, the spot diameter is 25 μm, and $S_n = 2.9\times10^3$ cm s^{-1} (from Ref. 26). With the passivating contribution of the AlGaAs shells, surface recombination dominates that from the interior volume of the NW (Ref. 26). Therefore, we obtain $\delta n_0 \approx G/S_n \approx 7.0 \times 10^{17}$ cm^{-3}. An inclusion of the contribution of volume recombination will result in an even lower value of δn.

[33] E.M. Gallo, G. Chen, M. Currie, T. McGuckin, P. Prete, N. Lovergine, B. Nabet, and J.E. Spanier, Appl. Phys. Lett. **98**, 241113 (2011).

[34] W.A. Tisdale, K.J. Williams, B.A. Timp, D.J Norris, E.S. Aydil, and X.Y. Zhu, Science **328**, 5985 (2010).

[35] R.T. Ross and A.T. Nozik, J. Appl. Phys. **53**, 3813 (1982).

[36] W. Shockley and H.J. Quiesser, J. Appl. Phys. **21**, 510 (1961).

FIG. 1: Schematic illustrations of (a) NW device configuration under illumination, and (b) electronic band diagram depicting real space transfer of photo-excited electrons from the NW core to the shell conduction bands under large E.

FIG. 2: Photocurrent-voltage traces, collected at 300K, for different values of (a) laser excitation wavelength demonstrating tunability (trace is normalized by peak current at V_{th} (*inset*: decrease of V_{th} for increasing laser excitation energy); (b) substrate gate bias V_g, as denoted in the legend (*inset*: the increase in V_{th} for larger negative gate voltages, demonstrating electrostatic gate tuning of V_{th}); and (c) incident optical intensity, as denoted in the legend (*inset*: dependence of V_{th} with incident optical intensity).

FIG. 3: (a) Measured nA-scale photocurrent response at 4.2K and under 0.33 mW Ti:S laser irradiation; (b) current at a fixed V_{bias} plotted as a function of T. The absence of a thermally-activated contribution to the photocurrent response over this range of T as seen in (b) indicates that scattering of photo-excited carriers by phonons is not significant.

FIG. 4: (a) Top: photocurrent traces for selected values of incident power: 14.1 mW (red), 9.7 mW (yellow), 5.2 mW (green), 3.9 mW (blue), and 2.85 mW (magenta); bottom: measured 2ω photocurrent signals associated with a small (250 mV) ac voltage modulation (50 Hz) bias applied to the NW about V_{th}; (b) demonstration of control of photocurrent phase with DC V_{bias} for fixed incident power. The vertical dashed red line denotes the value of V_{th} obtained from a DC I-V trace under identical intensity; and (c) top: arbitrary time series of incident light power selected to shift the value of V_{th} in relation to a fixed $V_{bias} = 2.4$V; bottom: corresponding 2ω signal, demonstrating optical amplitude modulation of non-linear response.

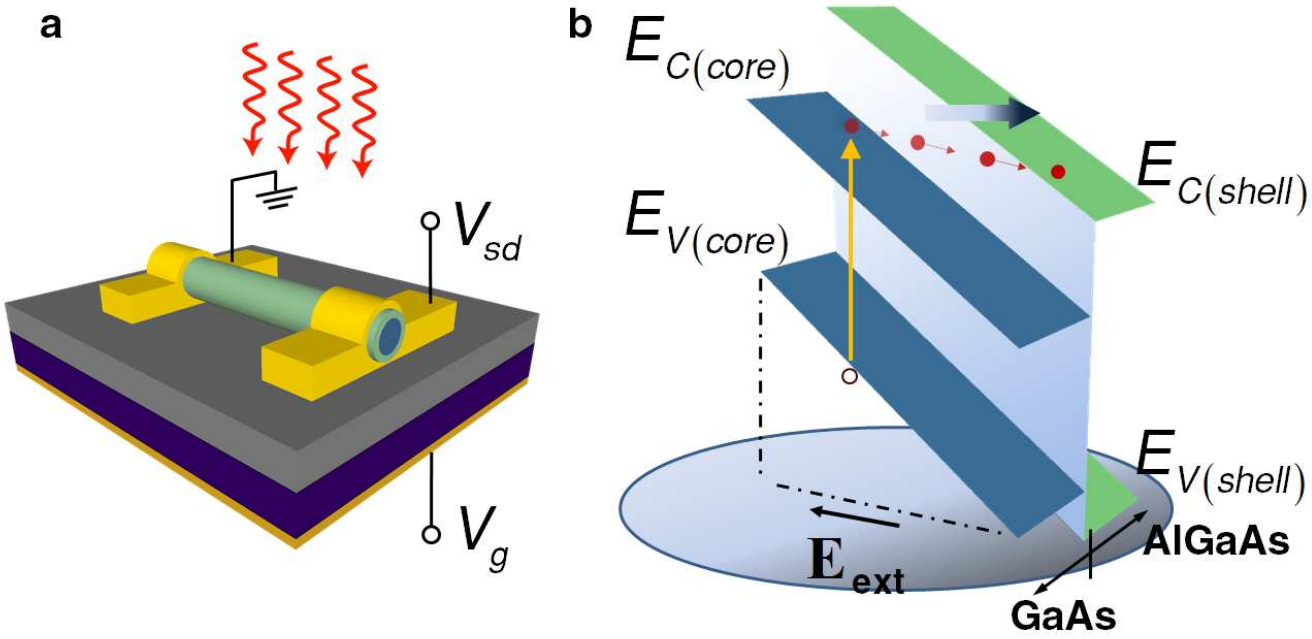

Figure 1 LC13992 08Aug2011

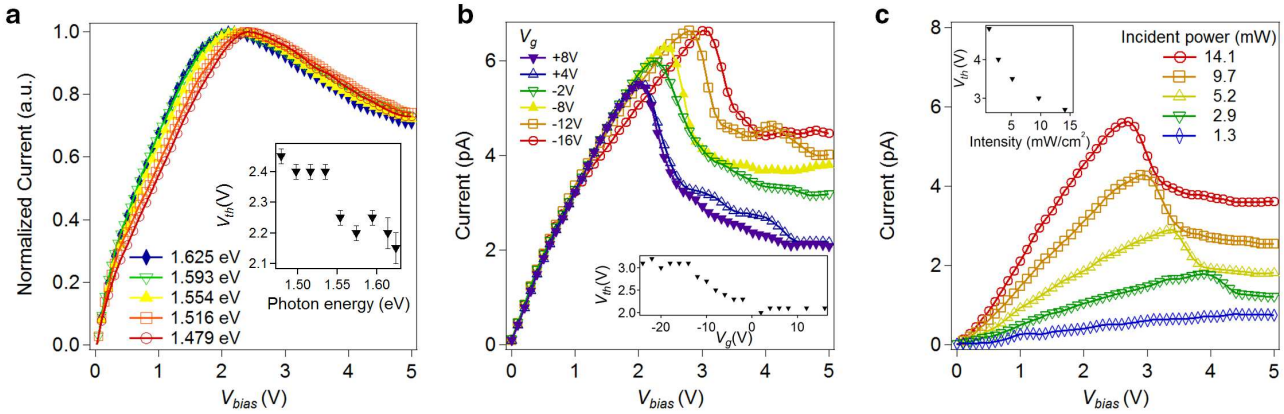

Figure 2 LC13992 08Aug2011

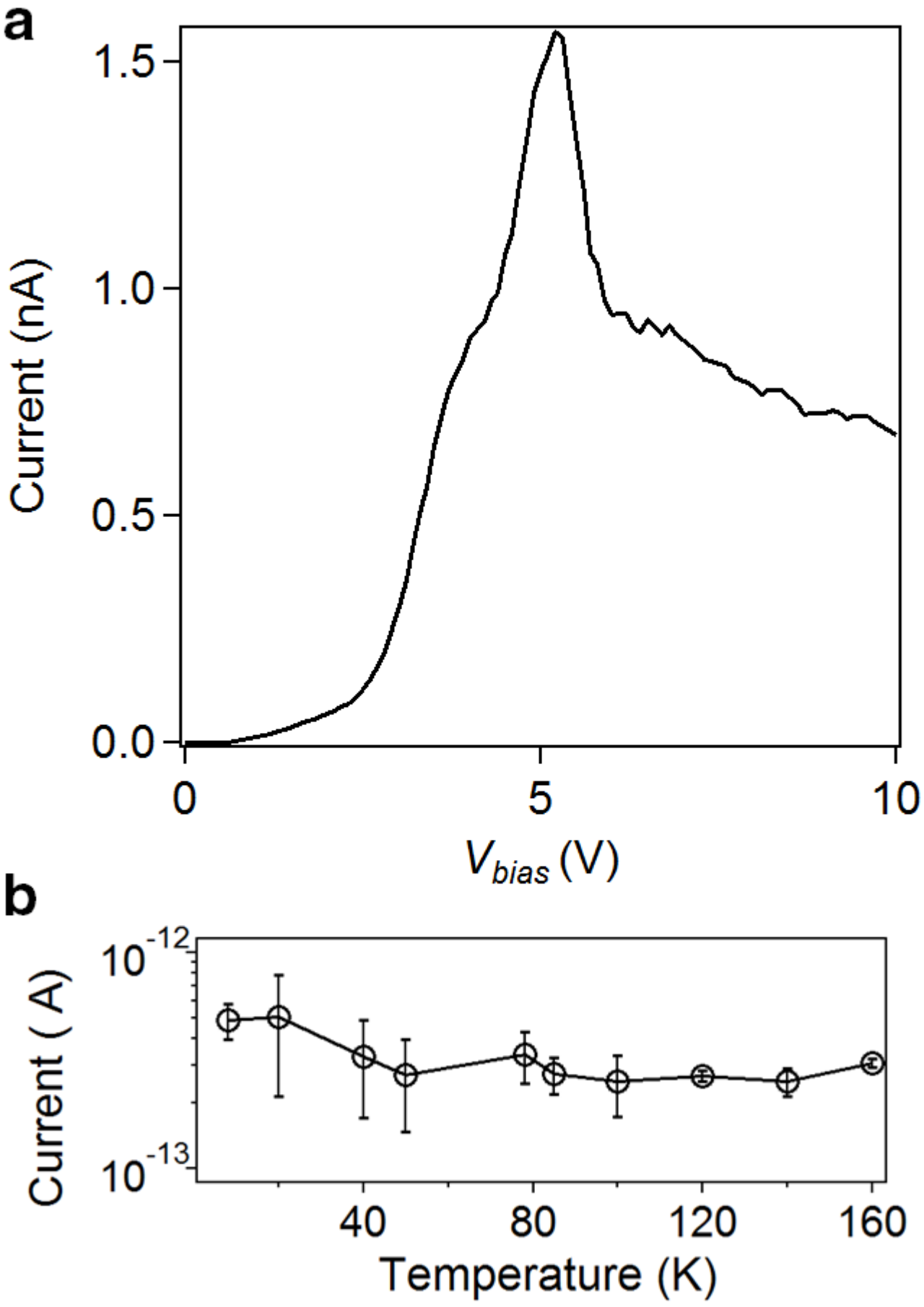

Figure 3 LC13992 08Aug2011

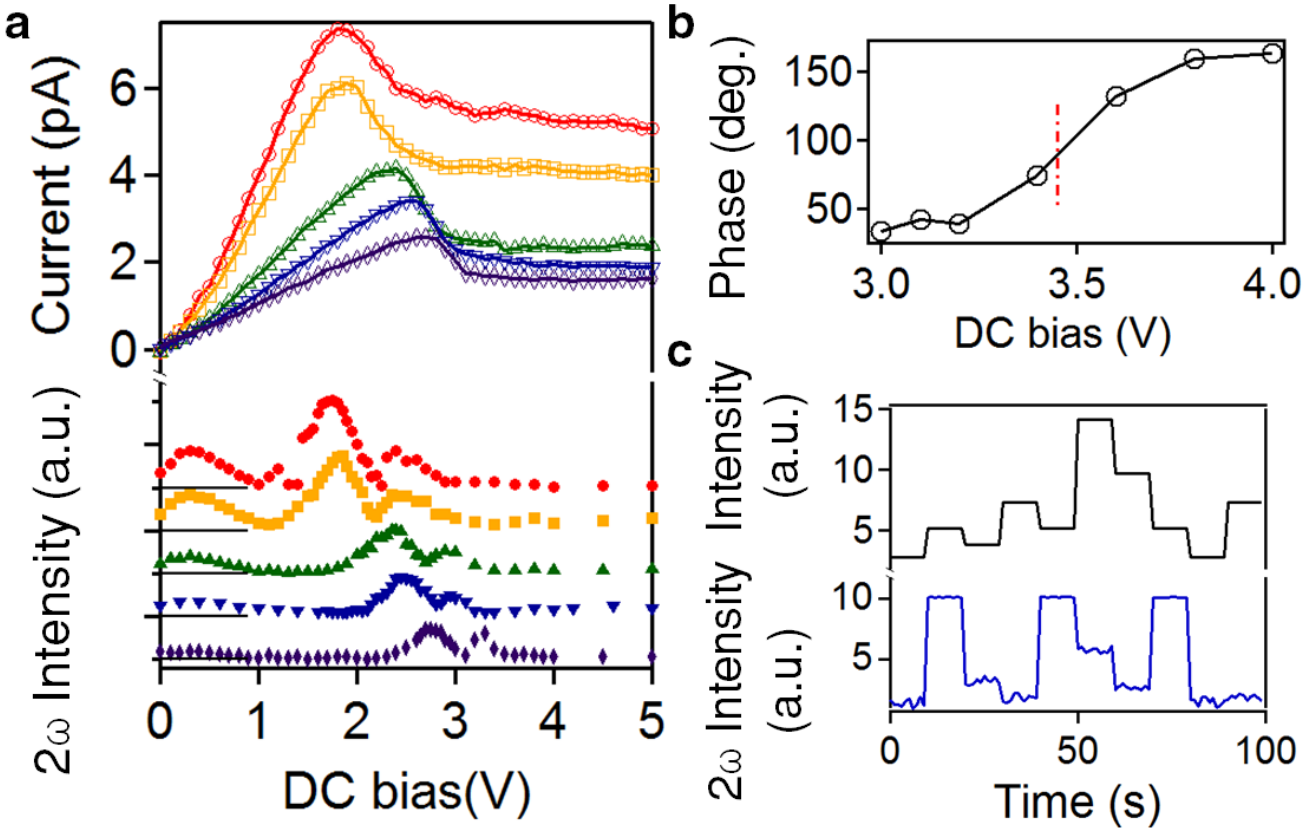

Figure 4 LC13992 08Aug2011